Scripta Materialia 166 (2019) 112–116

Contents lists available at ScienceDirect

Scripta Materialia

journal homepage: www.elsevier.com/locate/scriptamat

Radiation induced nanovoid shrinkage in Cu at room temperature: An *in situ* study

C. Fan [a], A.R.G. Sreekar [a], Z. Shang [a], Jin Li [a], M. Li [b], H. Wang [a,c], A. El-Azab [a,d], X. Zhang [a,*]

[a] School of Materials Engineering, Purdue University, West Lafayette, IN 47907, USA
[b] Nuclear Engineering Division, Argonne National Laboratory, Argonne, IL 60439, USA
[c] School of Electrical and Computer Engineering, West Lafayette, IN 47907, USA
[d] School of Nuclear Engineering, Purdue University, West Lafayette, IN 47907, USA

ARTICLE INFO

Article history:
Received 25 December 2018
Received in revised form 12 February 2019
Accepted 26 February 2019
Available online xxxx

Keywords:
Nanovoids
In situ radiation
Void shrinkage
Stacking fault tetrahedron
Phase-field modeling

ABSTRACT

Radiation induced void swelling is widely observed in a variety of metallic materials. Here, by using sputtering deposition technique, we have introduced faceted nanovoids into Cu films. *In-situ* Kr ion irradiation was subsequently performed at room temperature to investigate the evolution of nanovoids. Most nanovoids found to shrink gradually with increasing dose. Irradiation induced high-density vacancy clusters exist mostly in the form of stacking fault tetrahedrons. Phase field modeling reveales that void shrinkage arises from biased absorption of interstitials. These findings provide insights to the physical mechanisms of radiation response of nanovoids in metallic materials.

The irradiation of metallic materials with energetic particles creates atomic displacements in crystalline lattice and results in large concentrations of point defects, including vacancies and self-interstitial atoms (SIAs) [1]. The point defects then agglomerate into defect clusters, such as dislocation loops, stacking fault tetrahedrons (SFTs), and voids [2–6]. Such defects typically cause microstructural change and lead to significant degradation in the physical and mechanical properties of the irradiated material [7–10]. To design advanced radiation tolerant materials, it is essential to explore how such defect clusters evolve and interact with other defects during irradiation [11,12].

Irradiation-induced voids are of great interest for material performance, because they are directly related to volumetric swelling [13–18]. Extensive efforts have been devoted to investigating void formation and swelling mechanisms [19–21]. Experimentally, it has been demonstrated that void swelling behavior shows strong temperature dependence [22,23]. At low temperatures, void growth is limited by low vacancy mobility; at higher temperatures, however, void growth is suppressed by vacancy emission from voids [22] and accelerated vacancy-interstitial recombination [1]. Moreover, post-irradiation transmission electron microscopy (TEM) studies have revealed that the void morphology in irradiated metals often exhibits facets corresponding to low-index crystallographic planes [24]. For instance, irradiation-induced faceted voids have been reported in Ni [24], Mg [25], Cu [22], Cu—Ni alloys [26], and stainless steels [27]. However, *in situ* studies on void evolution under irradiation are still limited. Theoretically, the morphology evolution of voids is a complicated process, which involves thermodynamic factors of surface energy change and kinetic considerations governed by interfacial reactions [28–32]. Phase-field simulation can capture the morphological evolution of interfaces in various materials and recently it has been successfully applied for describing the void formation and evolution in irradiated metals [29–34].

In this study, we applied *in situ* TEM technique to investigate the evolution of faceted nanovoids in Cu under Kr ion irradiation at room temperature (RT). The nanovoids were introduced prior to irradiation, originating from the diffusion and collection of highly concentrated non-equilibrium vacancies during physical vapor deposition (PVD) process [35]. Our studies show that such nanovoids shrink and the aspect ratio of these irregular nanovoids also changes during radiation. It is hypothesized that the shrinkage and aspect ratio change of voids are primarily due to the dominant absorption of interstitials. We used the phase field modeling to gain insight on the role of interstitial in void evolution in irradiated Cu.

2-micron-thick Cu films were sputter-deposited on HF-etched Si (112) substrates at RT. The film texture was analyzed using an X-ray spectroscopy with a Cu $K\alpha_1$ source. Plan-view TEM specimens were prepared by polishing, dimpling and low-energy Ar ion-milling methods. TEM specimens were then irradiated with 1 MeV Kr ion beam up to a maximum fluence of 1×10^{14} ions/cm^2, at RT at the Argonne National Laboratory. More details regarding such *in-situ*

* Corresponding author.
E-mail address: xzhang98@purdue.edu (X. Zhang).

https://doi.org/10.1016/j.scriptamat.2019.02.046
1359-6462/

heavy ion irradiation technique have been reported and described elsewhere [36]. The Stopping and Range of Ions in Matter (SRIM) simulation with Kinchin-Pease method was used to estimate the radiation damage in unit of displacements-per-atom (dpa) [37,38]. According to SRIM simulation results, the maximum radiation damage was around 0.5 dpa with a constant dose rate ~0.003 dpa/s. Before and after irradiation the specimen was carefully examined by a Thermo Fischer Scientific/FEI Talos 200X microscope.

Conventional XRD profile in Fig. 1(a) shows the epitaxial growth of Cu (110) film on the Si (112) substrate. Plan-view TEM micrographs recorded at under-focus ($\Delta f = -1.5$ μm) and over-focus ($\Delta f = +1.5$ μm) conditions (Fig. 1(b–c)) reveal the formation of faceted nanovoids with dark and white Fresnel fringes. The inset selected area diffraction pattern in Fig. 1(b) confirms the formation of single-crystal-like Cu (110) film. The high-resolution TEM (HRTEM) image in Fig. 1(d) shows a typical nanovoid with facets on {111} planes and elongated along ⟨112⟩ direction. The length (L) and width (W) of such elongated nanovoids are measured as 17 ± 3 and 7 ± 2 nm, respectively.

Fig. 2(a–e) are sequential TEM snapshots at the same location that show the evolution of nanovoids under irradiation. As shown in Fig. 2(a), numerous defect clusters are formed surrounding pre-existing nanovoids at 0.1 dpa. During irradiation, these nanovoids shrank gradually. Some small nanovoids, as marked by arrows in Fig. 2(a) and (b), were eliminated beyond a certain dose level. Some large nanovoids, as marked by circles, survived the irradiation up to 0.5 dpa. The lower right insets in Fig. 2(a–e) show the enlarged views of a large nanovoid that contracted continuously during irradiation. It is worth mentioning that a large number of defect clusters in Fig. 2(e) are invisible, as the TEM specimen was tilted away from the standard zone-axis in order to reveal nanovoids. A tilted TEM micrograph in Fig. 2(f) examined along the ⟨110⟩ zone axis at a similar location clearly resolves a significant amount of defect clusters. More details corresponding to the radiation-induced void shrinkage can be found in supplementary video SV1.

Fig. 2(g–i) show the geometry variation for numerous nanovoids over 0.1–0.3 dpa. As shown in Fig. 2(g) and (h), both the length and width of nanovoids retract linearly with increasing dose, but the length reduces much more rapidly than the width (26 *vs.* 8 nm/dpa). For smaller nanovoids, such as the red triangular data points ($L = 9$ nm) in Fig. 2(i), the aspect ratio (W/L) increases from ~0.45 to 0.7. In contrast, for some larger nanovoids, such as the blue diamond data points ($L = 18$ nm) as shown in Fig. 2(f), the aspect ratio remains unchanged.

The image characteristics of irradiation-induced defect clusters depend sensitively on the diffraction conditions [6]. During irradiations some of the defects might be invisible because of sample drifting and tilting. To identify the irradiation-induced defect clusters, post-irradiation TEM analysis was performed. Fig. 3(a) is the bright-field TEM image that shows two remaining nanovoids surrounded by numerous SFTs. SFTs are a general type of 3-dimensional vacancy clusters in irradiated face-centered-cubic (FCC) metals with medium-to-low stacking fault energies [39]. Projected from ⟨110⟩ direction, they often have a triangular shape as confirmed by the HRTEM observation in Fig. 3(b). The average density of SFTs is ~5.5×10^{23}/m^3, and their average edge length (L_{SFT}) is ~2.4 nm, as shown in Fig. 3(c).

Radiation induced void swelling has been widely observed in irradiated metallic materials [19,20], and the magnitude of void swelling typically scales with radiation dose. The swelling rate is often greater for austenitic stainless steels (~1%/dpa) than that for ferritic/martensitic steels (~0.2%/dap) [40,41]. Swelling was not observed in the current study in Cu (110) with nanovoids. Instead nanovoids shrink continuously during radiation. In what follows we will briefly discuss the mechanisms of void shrinkage and the anisotropic nature of void shrinkage process.

The radiation effect on microstructural evolutions is determined by the kinetic and dynamic process of interstitials and vacancies and their clusters. Heavy ion irradiation creates equal numbers of interstitials

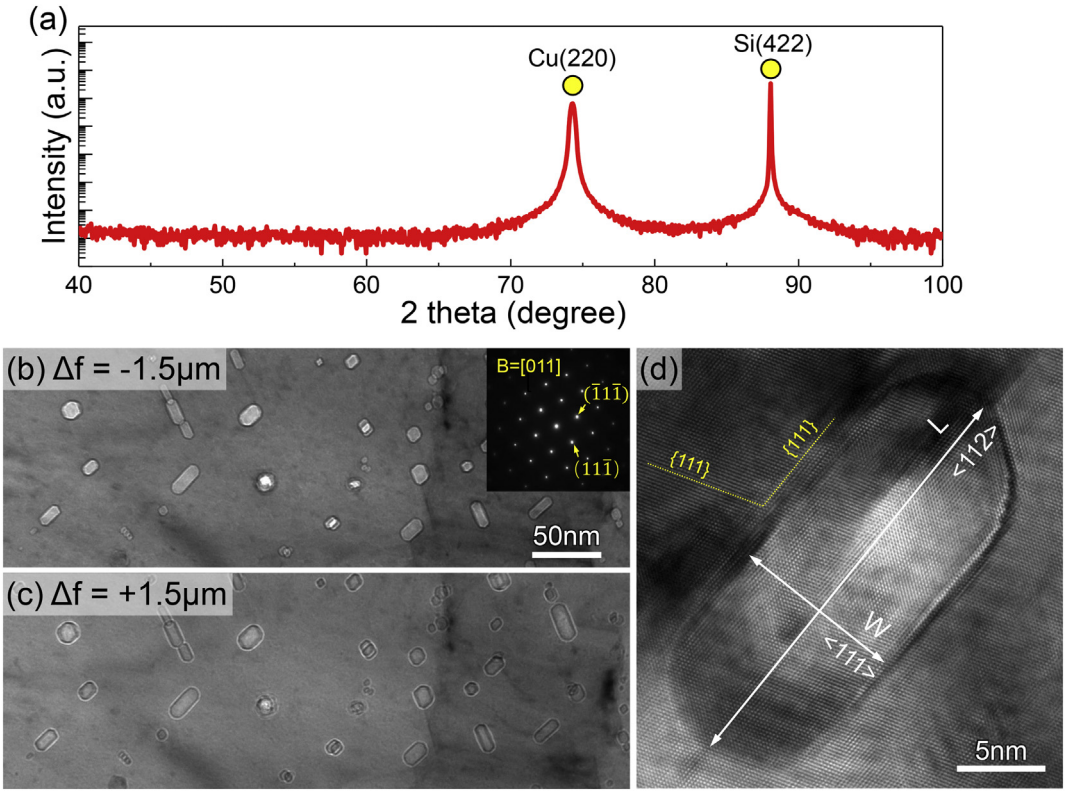

Fig. 1. Texture analysis, and microstructure characterization of as-deposited Cu (110) with nanovoids. (a) XRD pattern suggests the epitaxial growth of Cu (110) film on Si (112) substrate. (b–c) Plan-view TEM micrographs of faceted nanovoids in Cu films at under-focus and over-focus imaging conditions. (d) HRTEM image of a typical faceted nanovoid with the long side parallel to the {111} plane.

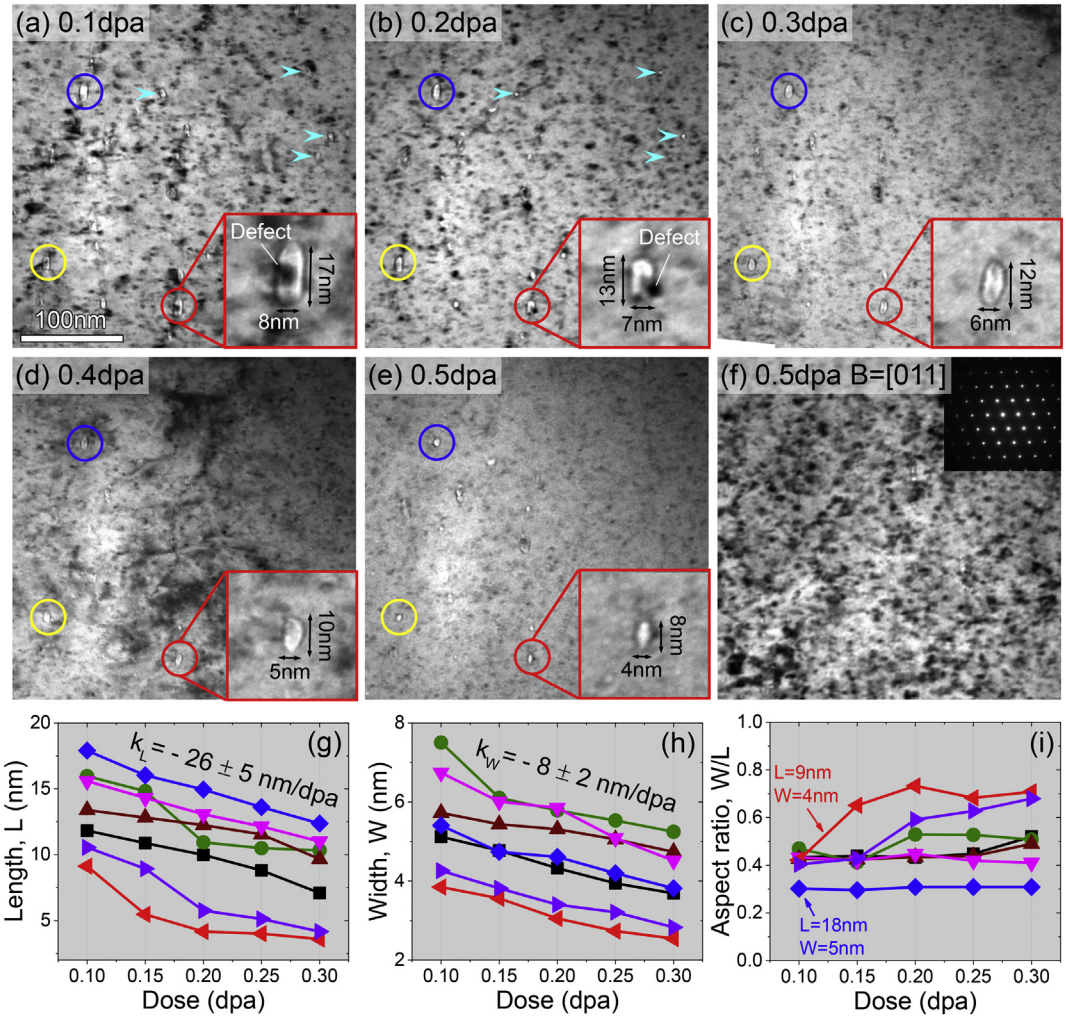

Fig. 2. (a–e) Sequential TEM snapshots revealing the void shrinkage (0.1–0.5 dpa). More details can be found in supplementary video SV1. (f) TEM micrograph taken at a similar position to panel (e) but along ⟨110⟩ zone axis reveals a significant number of defect clusters after irradiation to 0.5 dpa. (g–i) Dimension change of nanovoids with increasing dose.

and vacancies, and the interstitials are highly mobile at RT due to their low migration energy, ~0.12 eV for Cu [1]. Most of the radiation-induced interstitials would be annihilated through interstitial-vacancy recombinations within cascades [42]. The rest can escape from cascade damage zones and diffuse through the sample until they disappear at various sinks. Some of these free interstitials might be absorbed by free surfaces (top or bottom) of TEM foil, and others might diffuse into nanovoids and result in void shrinkage, as reported in irradiated nanovoid-nanotwinned Cu [43,44]. In comparison, vacancies have a high activation energy for migration, ~0.8 eV for Cu, and they become fully mobile only when temperature increases [1]. Therefore at room temperature, instead of long-range migrations, they exist in the form of SFTs [45], a type of sessile 3-dimensional vacancy clusters with a pyramidal configuration, as shown by their projection images in Fig. 3(b). It is

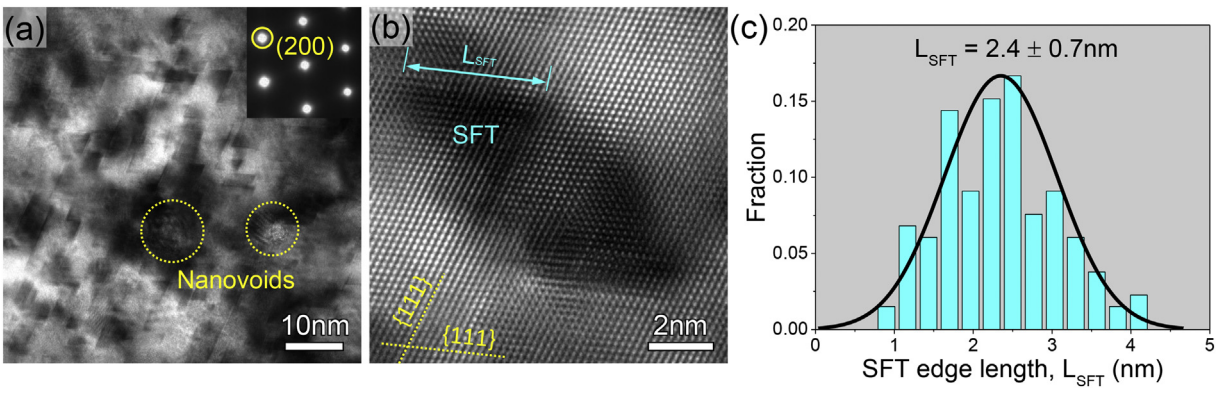

Fig. 3. (a–b) Post-irradiation TEM analysis identifying the defect clusters in the form of SFTs. (c) The statistic distribution of dimension of irradiation-induced SFTs.

worth noting that the SFTs could also act as point defect sinks and continuously grow or shrink by absorbing vacancies or interstitials. According to previous molecular dynamic studies, the interaction of point defects with a SFT is strongly dependent on its position and size [46]. The shrinkage or growth of SFTs is through the nucleation and movement of jogs along a face of tetrahedron. However, such processes are significantly suppressed for small tetrahedra at low temperature [46]. Our post irradiation analysis in Fig. 3 reveals that a high density of tiny SFTs remains in irradiated samples, indicating their high stability during their interactions with point defects. The free interstitials in current study, therefore, are assumed to be primarily absorbed by free surfaces of TEM foil or preexisting nanovoids.

To validate our hypothesis that the void shrinkage at RT is due to a biased absorption of interstitials, phase-field modeling was applied to determine the void evolution in Cu. The simulation was performed in two-dimensions with a thin film configuration as shown in Fig. 4(a). The model used was developed and reported elsewhere [47]. The simulation domain has 151 × 101 grid points in total, with the solid region occupying 101 × 101 grid points and the rest being empty space on both sides of the film. Two faceted nanovoids, with the same aspect ratio (0.4) but different sizes, are initialized at the center of the domains. The small void in Fig. 4(a) is 10 grid points long and 4 grid points wide, and the large void in Fig. 4(b) is 40 grid points long and 16 grid points wide. The concentration of point defects is initially taken to be equal to the thermal equilibrium concentration. To model the low temperature irradiation scenario, the following ratio of point defect diffusivities is assumed: $D_i/D_v = 60$. This ratio, which indicates that interstitial mobility is much higher than vacancy mobility, is consistent with the diffusion of vacancies and interstitials in FCC metals at low temperature [32]. In order to account for the observed SFTs, the free defects introduced by cascade damage are assumed to follow a biased cascade source – namely, the number of vacancies introduced in each cascade is 90% of the number of interstitials. The surface energy anisotropy on void shrinkage is also included in the simulation model by making the gradient coefficient of the non-conserved order parameter orientation-dependent, as what has been reported in another study [33]. More detailed information about the phase-field simulation of irradiated metals can be found elsewhere [29,31].

Fig. 4 depicts the simulation results on void shrinkage under irradiation. At low temperature, as freely migrating interstitials have higher concentration and greater diffusivity than vacancies, they rapidly diffuse towards the void and deposit at the void surface. As such, the preexisting void shrinks gradually as shown in Fig. 4(a–g). Fig. 4(h–j) present the evolution of void dimension and geometry with time during radiation. Fig. 4(h) indicates the small void shrinks much faster than the large one. Note that the void length reduction rate in Fig. 4(i) is higher than width reduction rate. Consequently, the void aspect ratio in Fig. 4(f) increases immediately for the small void. In contrast, the large void initially increases slowly in aspect ratio, but in later stages it rapidly becomes spherical when the void size reduces further. More details regarding the phase field modeling of void evolution can be found in supplementary videos SV2 and SV3. These simulation results agree qualitatively with our experimental observations (see Fig. 2).

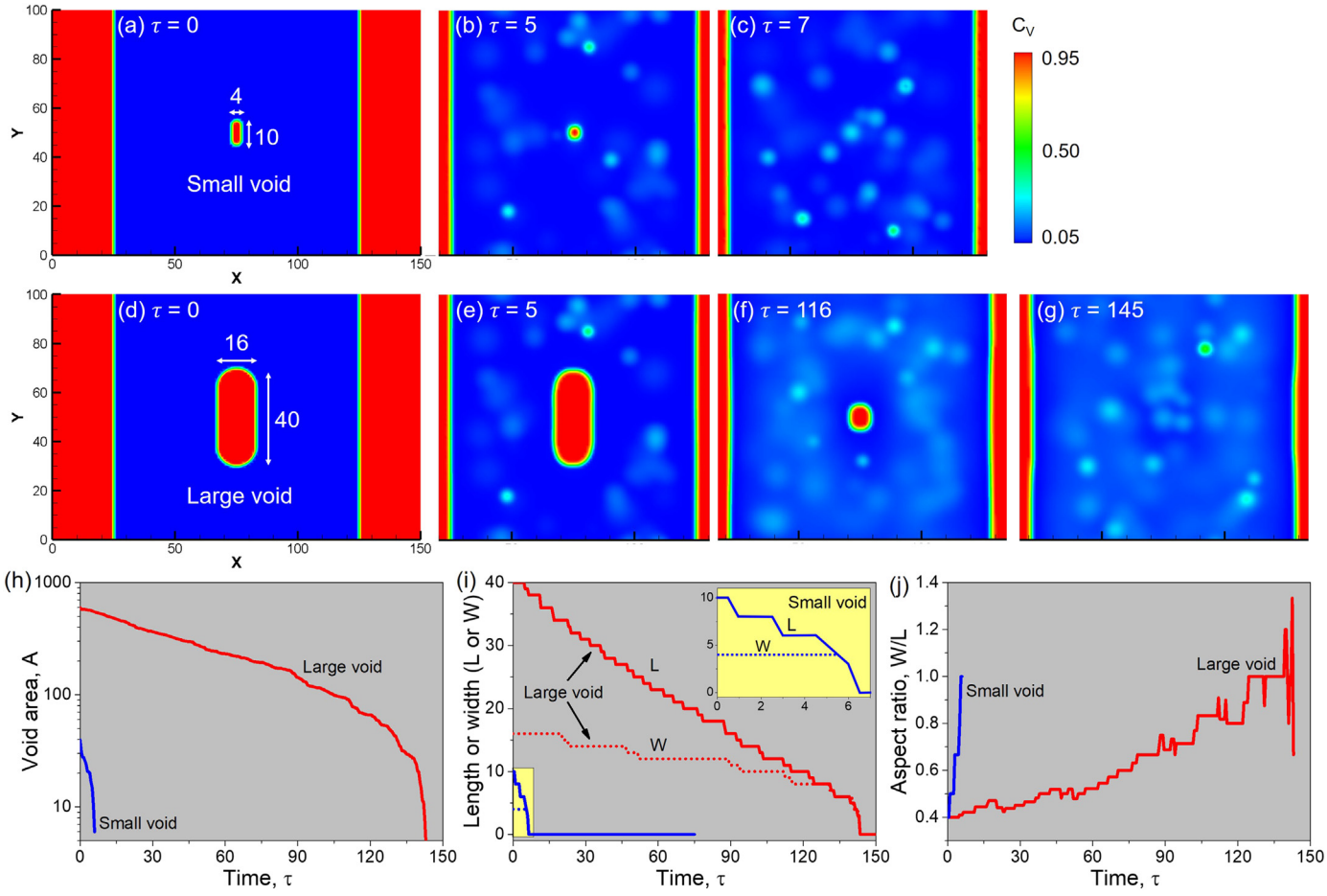

Fig. 4. Phase-field simulations on the radiation-induced void shrinkage due to a supersaturated self-interstitial concentration at low temperature. (a–g) The evolution of vacancy concentration for a small void in (a–c) and a large void in (d–g). More details can be found in supplementary videos SV2 and SV3. (h–j) Radiation-induced geometrical evolution for the small (blue lines) and large (red lines) void. (h) The reduction of void area (A, in logarithmic). (i) The reduction of void width (W, dotted lines) and length (L, solid lines). (j) The increment of void aspect ratio (W/L). (For interpretation of the references to colour in this figure legend, the reader is referred to the web version of this article.)

We now examine the anisotropic shrinkage of nanovoids. *In situ* radiation studies show that the void length shrinks much faster than void width and eventually radiation leads to spheroidization of nanovoids. The anisotropy is primarily attributed to the effect of void surface curvature. As shown in Fig. 1(d), the elongated nanovoids are primarily faceted on {111} side walls that have little curvature, while both ends of the voids have a large curvature. The equilibrium interstitial concentration (C_i^{eq}) at the surface can be described by [48]:

$$C_i^{eq} = e^{-\frac{E_i^f + \Omega\kappa\gamma}{k_B T}} \quad (1)$$

where κ is the void surface curvature (with positive sign) that equals the reciprocal of the radius for a spherical void, E_i^f is the interstitial formation energy, Ω is the atomic volume, γ is the surface energy, k_B is the Boltzmann constant, and T is the temperature. The equation indicates that the increase in surface curvature decreases the equilibrium concentration of interstitials at the surface, thus accelerating the diffusion of interstitials to the region of void surfaces with larger curvatures and leading to biased shrinkage (spheroidization) of elongated voids.

Given the curvature's effect on promoting spheroidization, one would anticipate that during radiation, most nanovoids should spheroidize first rapidly and then shrink during irradiation. However, our *in-situ* observations in Fig. 2 show that large nanovoids (with L > ~15 nm) remain their lenticular shape during shrinkage, whereas spheroidization appears to occur faster in voids with smaller L (~10 nm or less). It is likely that the surface tension of smaller nanovoids is greater than that of larger nanovoids, and hence surface tension accelerates the spheroidization of small nanovoids. Chen et al. have shown that smaller nanovoids shrink faster in nanotwinned Cu as the tensile stress near the void surface is high [43]. The spheroidization process may also be accelerated at elevated temperatures when the surface mobility increases significantly. However, at elevated temperatures, the void shrinkage rate may decrease. Such a hypothesis requires further experimental validation in our future studies. But recent studies on temperature dependent shrinkage of nanopores in nanoporous Au suggest that higher temperature can indeed reduce the shrinkage rate of nanopores [5].

A fundamental understanding of void evolution is crucial for the design of advanced radiation tolerant materials with outstanding void swelling resistance. *In situ* TEM irradiation studies of Cu with nanovoids, performed at room temperatures, show that preexisting elongated and faceted nanovoids shrink continuously during irradiation. Small nanovoids spheroidize rapidly during radiation, whereas large nanovoids appear to maintain their aspect ratio during shrinkage. The shrinkage mechanism is ascribed to the supersaturated interstitials, while the less mobile vacancies cluster into SFTs. The variation of void aspect ratio is related to the anisotropic diffusion of interstitials into nanovoids and the surface tension of voids.

Supplementary data to this article can be found online at https://doi.org/10.1016/j.scriptamat.2019.02.046.

Acknowledgements

We acknowledge financial support by NSF-CMMI-1728419. C. Fan is also supported by Bilsland Dissertation Fellowship at Purdue University. Z. Shang is supported by NSF-DMR-Metallic Materials and Nanostructures Program under grant. 1611380. H. Wang acknowledges the support from the U.S. Office of Naval Research (N00014-16-1-2778).

References

[1] G.S. Was, Fundamentals of Radiation Materials Science: Metals and Alloys, Springer, 2016.
[2] S. Zinkle, Comprehensive Nuclear Materials, Elsevier, Oxford, 2012 65–98.
[3] S. Zinkle, R. Sindelar, J. Nucl. Mater. 155 (1988) 1196–1200.
[4] J. Li, C. Fan, J. Ding, S. Xue, Y. Chen, Q. Li, H. Wang, X. Zhang, Sci. Rep. 7 (2017).
[5] J. Li, C. Fan, Q. Li, H. Wang, X. Zhang, Acta Mater. 143 (2018) 30–42.
[6] M. Jenkins, J. Nucl. Mater. 216 (1994) 124–156.
[7] T.D. de la Rubia, H.M. Zbib, T.A. Khraishi, B.D. Wirth, M. Victoria, M.J. Caturla, Nature 406 (6798) (2000) 871.
[8] M. Victoria, N. Baluc, C. Bailat, Y. Dai, M. Luppo, R. Schaublin, B. Singh, J. Nucl. Mater. 276 (1–3) (2000) 114–122.
[9] S. Zinkle, G. Kulcinski, L. Mansur, J. Nucl. Mater. 141 (1986) 188–192.
[10] K. Yu, Y. Liu, C. Sun, H. Wang, L. Shao, E. Fu, X. Zhang, J. Nucl. Mater. 425 (1) (2012) 140–146.
[11] X. Zhang, K. Hattar, Y. Chen, L. Shao, J. Li, C. Sun, K. Yu, N. Li, M.L. Taheri, H. Wang, Prog. Mater. Sci. 96 (2018) 217–321.
[12] S.J. Zinkle, G. Was, Acta Mater. 61 (3) (2013) 735–758.
[13] M. Cambini, J. Bressers, M. Heerschap, J. Nucl. Mater. 62 (2–3) (1976) 311–313.
[14] J. Evans, J. Nucl. Mater. 88 (1) (1980) 31–41.
[15] D. Gelles, J. Nucl. Mater. 225 (1995) 163–174.
[16] E. Little, D. Stow, J. Nucl. Mater. 87 (1) (1979) 25–39.
[17] B. Singh, A. Horsewell, D. Gelles, F. Garner, J. Nucl. Mater. 191 (1992) 1172–1176.
[18] C. Cawthorne, E. Fulton, Nature 216 (5115) (1967) 575–576.
[19] A. Brailsford, R. Bullough, J. Nucl. Mater. 44 (2) (1972) 121–135.
[20] L.K. Mansur, Nucl. Technol. 40 (1) (1978) 5–34.
[21] R. Bullough, B. Eyre, K. Krishan, Proc. R. Soc. Lond. A 346 (1644) (1975) 81–102.
[22] S.J. Zinkle, K. Farrell, J. Nucl. Mater. 168 (3) (1989) 262–267.
[23] S. Zinkle, K. Farrell, H. Kanazawa, J. Nucl. Mater. 179 (1991) 994–997.
[24] C. Chen, Phys. Status Solidi A 16 (1) (1973) 197–210.
[25] W. Xu, Y. Zhang, G. Cheng, W. Jian, P.C. Millett, C.C. Koch, S.N. Mathaudhu, Y. Zhu, Nat. Commun. 4 (2013) 2288.
[26] S. Zinkle, B. Singh, J. Nucl. Mater. 283 (2000) 306–312.
[27] P. Maziasz, J. Nucl. Mater. 169 (1989) 95–115.
[28] P. Goodhew, Met. Sci. 15 (9) (1981) 377–385.
[29] P.C. Millett, A. El-Azab, S. Rokkam, M. Tonks, D. Wolf, Comput. Mater. Sci. 50 (3) (2011) 949–959.
[30] P.C. Millett, A. El-Azab, D. Wolf, Comput. Mater. Sci. 50 (3) (2011) 960–970.
[31] S. Rokkam, A. El-Azab, P. Millett, D. Wolf, Model. Simul. Mater. Sci. Eng. 17 (6) (2009), 064002.
[32] P.C. Millett, S. Rokkam, A. El-Azab, M. Tonks, D. Wolf, Model. Simul. Mater. Sci. Eng. 17 (6) (2009), 064003.
[33] W. Liu, N. Wang, Y. Ji, P. Song, C. Zhang, Z. Yang, L. Chen, J. Nucl. Mater. 479 (2016) 316–322.
[34] Z. Xiao, A. Semenov, C. Woo, S. Shi, J. Nucl. Mater. 439 (1) (2013) 25–32.
[35] G. Zhigal'Skii, B.K. Jones, The Physical Properties of Thin Metal Films, CRC Press, 2003.
[36] M. Li, M. Kirk, P. Baldo, D. Xu, B. Wirth, Philos. Mag. 92 (16) (2012) 2048–2078.
[37] J.F. Ziegler, M.D. Ziegler, J.P. Biersack, Nucl. Instrum. Methods Phys. Res., Sect. B 268 (11) (2010) 1818–1823.
[38] R.E. Stoller, M.B. Toloczko, G.S. Was, A.G. Certain, S. Dwaraknath, F.A. Garner, Nucl. Instrum. Methods Phys. Res., Sect. B 310 (2013) 75–80.
[39] R. Schäublin, Z. Yao, N. Baluc, M. Victoria, Philos. Mag. 85 (4–7) (2005) 769–777.
[40] C. Sun, S. Zheng, C. Wei, Y. Wu, L. Shao, Y. Yang, K. Hartwig, S. Maloy, S. Zinkle, T. Allen, Sci. Rep. 5 (2015) 7801.
[41] M. Song, Y. Wu, D. Chen, X. Wang, C. Sun, K. Yu, Y. Chen, L. Shao, Y. Yang, K. Hartwig, Acta Mater. 74 (2014) 285–295.
[42] M. Kiritani, T. Yoshiie, S. Kojima, J. Nucl. Mater. 141 (1986) 625–632.
[43] Y. Chen, K.Y. Yu, Y. Liu, S. Shao, H. Wang, M. Kirk, J. Wang, X. Zhang, Nat. Commun. 6 (2015).
[44] C. Fan, Y. Chen, J. Li, J. Ding, H. Wang, X. Zhang, J. Nucl. Mater. 496 (2017) 293–300.
[45] S. Zinkle, L. Seitzman, W. Wolfer, Philos. Mag. A 55 (1) (1987) 111–125.
[46] Y.N. Osetsky, A. Serra, M. Victoria, S. Golubov, V. Priego, Philos. Mag. A 79 (9) (1999) 2285–2311.
[47] A. El-Azab, K. Ahmed, S. Rokkam, T. Hochrainer, Curr. Opinion Solid State Mater. Sci. 18 (2) (2014) 90–98.
[48] T. Hochrainer, A. El-Azab, Philos. Mag. 95 (9) (2015) 948–972.